# RSC Advances

This is an *Accepted Manuscript*, which has been through the Royal Society of Chemistry peer review process and has been accepted for publication.

*Accepted Manuscripts* are published online shortly after acceptance, before technical editing, formatting and proof reading. Using this free service, authors can make their results available to the community, in citable form, before we publish the edited article. This *Accepted Manuscript* will be replaced by the edited, formatted and paginated article as soon as this is available.

You can find more information about *Accepted Manuscripts* in the **Information for Authors**.

# Recent Advances in Metal-Organic Frameworks based on Pyridylbenzoate Ligands: Properties and Applications

Gift Mehlana*, Vitalis Chitsa and Tawanda Mugadza

*Midlands State University, Department of Chemical Technology, Private Bag 9055 Senga Road, Gweru, Zimbabwe*

*E-mail: mehlanag@msu.ac.zw,*

### Abstract

In this mini review, a summary of metal-organic frameworks (MOFs) assembled using 3-(4-pyridyl)benzoate (34pba) and 4-(4-pyridyl)benzoate (44pba) is presented. These materials exhibit interesting properties such as negative and positive thermal expansion, breathing behaviour, solvatochromism/vapochromism, thermochromism luminescence and exceptional iodine capture. Throughout the review we discuss the properties exhibited by MOFs constructed from the 44pba and 34pba linkers and we also highlight some of the exceptional behaviour of these materials.

### 1. Introduction

The design and synthesis of porous MOFs have attracted considerable attention due to their intriguing structures and their potential applications in the fields of sensing, switching, storage, catalysis and photoluminescence.[1-6] The use of ligands with mixed donor atoms in the construction of coordination polymers is of current interest owing to the formation of various coordination polymers with special topologies and useful functionalities. MOFs are crystalline materials that contain extended networks constructed by the linkage of metal ions by multiply-coordinating polydentate ligands.[7,8] The simplest ligands within the family of mixed nitrogen, oxygen donors are pyridine monocarboxylic acid that comprise of pyridine and carboxylate functionalities. There exist three isomers, which are 4-pyridine carboxylic acid, 3-pyridine carboxylic acid, and 2-pyridine carboxylic acid. The ligand isonicotic acid is considered to be the most straight forward and a fundamental case. The ligand is unsymmetrical and linear combing the characteristics of 4'4-bipyridine and terephthalic acid which are employed in the design and construction of MOFs.

In this review we mainly focus on MOFs based on pyridylcarboxylate linkers of 34pba and 44pba (Figure 1). For a detailed review on MOFs based on pyridylcarboxylates readers are encouraged to read a review by Yan Lin *et al.*[9] Early work by Robson and co-workers involved the use of 4,4'-bipyridine linkers to construct materials which he referred to as coordination polymers. A search in the Cambridge structural database shows that there are over 5600 (2015 update) compounds assembled from 4,4'bipyridine linkers. Yaghi and co-works used compounds with the carboxylate moiety to synthesise porous materials and he referred them as MOFs although Yaghi's earlier definitions of a MOF encompassed compounds based on M-N linkages[10]. Carboxylate groups are expected to form strong coordination bonds with metal ions while the nitrogen to metal bonds is generally weak. MOFs assembled from these 44pba and 34pba inherit early aspects of Robson's coordination polymers based on 4,4-bipyridine and the carboxylate MOFs, such as Yaghi's MOF-5.[11] This is why the terminology in this field of study needs to be inclusive rather than restrictive.[8,12] Asymmetrical ligands have gained considerable attention because they are prototypes for supramolecular self-assembly processes including metal-organic helices.[13,14] 44pba is an asymmetrical ditopic organic linker comprising of the pyridyl and carboxylate moieties which are both capable of binding to the metal centre to afford extended networks. The different binding modes that can be assumed by the carboxylate moiety make it easy to obtain diverse structures with different physical and chemical properties Several crystal structures with different topologies and interesting properties have been prepared using this ligand.[4-15] One limitation of using long linkers such as 44pba in the self-assembly of MOFs is the formation of interpenetrated networks which reduces the porosity of the material.

The presence of the pyridyl and carboxylate groups in these linkers may give rise to secondary building units of high connectivity which may not be observed when using non pyridylcarboxylate linkers. Studies by Zhang and co-workers have revealed that a combination of 44pba and naphthalenedicarboxylates (ndc) produced a porous metal carboxylate framework, $[Ni^{II}_2Ni^{III}(\mu_3\text{-OH})(44pba)_3(ndc)_{1.5}]$ (MCF-19), constructed from the $Ni_3(\mu_3\text{-OH})(O_2CR)_6(L^1)_3$ clusters. The network has an unprecedented, uninodal, nine-connected **ncb** topology with a unique hierarchical channel-cavity biporous system.[16,17] Just like the 44pba, the labile conformations and coordination modes of 34pba play a key role in the construction of various structures which can be achieved by varying the synthetic conditions. Furthermore, different network connectivity and porosities can be realised depending on the shape and the bridging angles of the ligand.[18] Zhou *et al* studied the energy profiles of the 34pba ligand.[19] The potential energy of the 34pba at different conformations was calculated using the density functional theory. It was found that the 34pba has two stable conformations of +35.8° and -35.8° between the pyridyl and

phenyl ring which are separated by an energy barrier of 6.3 kJ·mol^{-1}. The low difference in the energy barrier indicates that the 34pba ligand can easily undergo reversible conformation change under external stimuli.
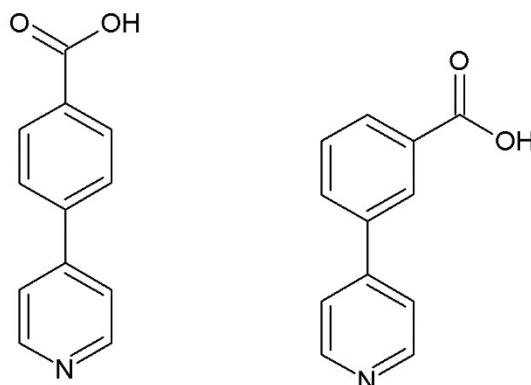


**Fig 1:** Linkers discussed in this review, left: 4-(4-pyridyl)benzoic acid and right: 3-(4-pyridyl)benzoic acid

Unlike other linear linkers, the 34pba is able to vary its length as a result of the change in the binding mode of the carboxylate, for example a change from the chelating binding mode to monodentate results in the lengthening of the bend ligand and vice versa. Such behaviour may be exploited for the design and construction of materials with unprecedented positive and negative thermal expansion properties.

**2.0  General Synthetic Methods**

Majority of MOFs assembled from 34pba and 44pba were synthesised using the solvothermal approach. This technique gives rise to the formation of highly porous MOFs. The method involves dissolving the metal salt and ligands in an appropriate solvent followed by heating the reactants at temperatures below 120 °C in a tightly sealed autoclave. Dimethylformamide is normally employed in this technique as it can facilitate deprotonation of the carboxylic acid group. Varying of reaction temperatures under solvothermal conditions has been employed  to yield different superstructures.[12] Hydrothermal synthesis has also been used to assemble MOFs of 34pba and 44pba. This technique involves adding the reactants in an autoclave with an appropriate amount of water. The reactants are heated at temperatures above 150 °C for a certain period of time before cooling to room temperature. The disadvantage of hydrothermal synthesis when using long linkers is that it normally gives rise to highly interpenetrated networks, [20,21] due to the solvent molecules playing a templating role. Water being a small molecule gives rise to small pores as the other void space will be occupied by the interpenetrating networks. Hydrothermal synthesis has been reported to be the most effective method of preparing MOFs based on mixed ligands.[9] This is because under hydrothermal conditions, the viscosity of water is reduced which enhances the diffusion processes and thus extraction of solids and crystal growth from solution is favoured. Solvent evaporation has also been employed to produce MOFs of 34pba and 44pba. This method involves dissolving the reacting components in a suitable solvent or a mixed solvent system. The resulting solution is placed in a vial and the solvent allowed to evaporate at room temperature. The disadvantage of this method is that the fluctuation of the room temperature makes it very difficult to reproduce the materials, since MOFs synthesis is very sensitive to slight changes in the reaction conditions. Table 1 lists the properties of various MOFs assembled from the 34pba and 44pba linkers.

Table 1: A summary of MOFs made using the 34pba and 44pba linkers

| | Molecular Formula | Topology | Properties | Reference |
|---|---|---|---|---|
| **MOFs of 34pba** | [ $Zn(34pba)_2]_n$ | **sql** | breathing, seperation of alcohols | [22] |
| | {[$Zn(34pba)_2]\cdot 0.5DMF\cdot 0.5H_2O\}_n$ | **sql** | High affinity of alcohols | [23] |
| | [$Zn_2(OH)(L)_3]_n$ | - | photoluminescence | [24] |
| | [$Ni(L)_2(C_2H_6O_2)]_n$ | - | photoluminescence | [24] |
| | [$Fe_2(OH)(L)_3]_n$ | - | photoluminescence | [24] |
| | [$Ni(L)_2(H_2O)]_n$ | - | photoluminescence | [24] |
| | [$Cd(L)_2(H_2O)]_n$ | - | photoluminescence | [24] |
| | [$Mn(34pba)_2]_n$ | **ant** | positive and negative thermal expansion | [19] |
| | [$Co(34pba)_2\cdot DMF\}_n$ | **bcu** | thermochromic and solvatochromic | [12] |
| | {[$Co(34pba)_2]\cdot DMF\}_n$ | **sql** | thermochromic | [12] |
| | [$Co(34pba)_2\cdot(H_2O)_4]_n$ | | thermochromic and mechanochromic | [25] |
| **MOFS of 34pba with axulliary ligands** | [$Co_2(OH)(3,4\text{-}PBC)_3]_n$ | - | antiferromagnetic | [26] |
| | [$Cd(34pba)(44pba)]_n$, | **bcu** | positive and negative thermal expansion | [27] |
| **MOFs of 44pba** | [$LnCuL_4][Ln_{0.25}Cu_{0.25}L]_n$ | **dia and mdf** | luminescence | [28] |
| | {[$Mn(44pba)_2]\cdot 2.5DMF\}_n$ | **rtl** | positive and negative thermal expansion | [18] |
| | {[$Co(II)(pybz)_2]\cdot 2DMF\}_n$ | **dia** | vapochromism | [29] |
| | {[$Co_4(44pba)_8]\cdot 3DMF\cdot 0.25EtOH\cdot 4H_2O\}_n$ | **dia** | solvatochromism | [30] |
| | {[$Co_2(44pba)_4 (MeOH)_2]\cdot (MeOH)_{2.5}\cdot (H_2O)_2\}_n$ | **pts** | solvatochromic | [31] |
| | {[$Co(44pba)_2 (MeOH)_2]\cdot (MeOH)_{0.5}(H_2O)_{0.5}\}_n$ | **quartz** | solvatochromic | [31] |
| **MOFs of 44pba with axulliary ligands** | [$Co_3(pybz)_2(pico)_2]_n$ | **bcu** | ferrimagnetic | [32] |
| | {[$Co^{II}_3(lac)_2(pybz)_2]\cdot 3DMF\}_n$ | - | magnetism | [33] |
| | {[$Cu_2(44pba)_3(N_3)]\cdot 3H_2O\}_n$ | - | ferromagnetic | [34] |
| | [$Mn(44pba)(N_3)(H_2O)_2]_n$ | - | antiferromagnetic | [34] |
| | [$Cd(34pba)(44pba)]_n$ | **bcu** | positive and negative thermal expansion | [27] |
| | {[$Zn_3(dl\text{-}lac)_2(pybz)_2]\cdot 3DMF\}_n$ | - | exceptional iodine capture | [4] |
| | {[$Cu_6(pybz)_8(OH)_2]\cdot I_5\cdot I_7\}_n$ | - | | [15] |
| | [$Ni^{II}_2Ni^{III}(\mu_3\text{-}OH)(44pba)_3(ndc)_{1.5}]_n$ | **nbo** | Moderate methane affinity | [16, 17] |
| | {[$Zn_2 (44pba)_2 (BDC)]\cdot (DMF)_3 (H_2O)_4\}_n$ | **pcu** | Separation of $C_2H_6$, $C_2H_4$, and $C_2H_2$ over $CH_4$ | [35] |

L = 34pba or 44pba, pico = 3-hydroxypicolinate, 3,4-PBC = 34pba, pybz = 44pba, dl-lac = lactate, MeOH = methanol, ndc = naphthalenedicarboxylates, BDC = biphenyldicarboxylate

### 3.0 Breathing effects in 2D MOFs of pyridylcarboxylates

Breathing is an interesting phenomenon that has been observed in several MOFs. During breathing, the displacement of atoms of the framework is accompanied by a change in the unit cell volume. Several kinds of guest-induced structural flexibility have been reported, including "gate-opening" or "breathing" behaviour. Recently a great number of studies have been devoted towards understanding the breathing phenomenon in MOFs and some studies have highlighted the thermodynamic basis for such behaviour.[36] Dynamic breathing movement in MOFs may happen through a displacive phase transition, DPT (without bond breaking) or a reconstructive phase transition RPT (including bond breaking).[37] The latter is uncommon and includes creation of open metal sites which can be used for catalytic applications. During the breathing

transitions between large pores (**lp**) and narrow pores (**np**) the crystallographic space groups may change. A recent review by Ferey *et al* outlined some of the empirical requirements of breathing in 3D compounds assembled from organic linkers and secondary building units (SBU).[37] They reported that SBU which permit breathing are those which possess a mirror plane with the carboxylates in symmetrical position with respect to the mirror plane. He further points out that only ditopic carboxylate ligands can allow breathing. This is because between two SBU metal clusters the kneecaps provided by the O...O axes of the different carboxylate ought to be parallel for possible phase rotations. This condition inhibits the use of tri- or tetratopic ligands for expecting swelling which is the case of MOF-77,[38] MIL-103,[39] which contain tritopic 1,3,5-benzene trisbenzoate and MIL-102[40] formed with the naphthalene 1,4,5,8-tetracarboxylate.

### 3.1 Breathing of MOFs based on 34pba ligands

MOFs composed of 2D interdigitated layers which are of interest as the ability of the 2D layers to glide past each other allows for the accommodation of large guest molecules with diameters larger than the initial pores of framework.[41,42] Such motion of the 2D layers is normally triggered by the $\pi \cdots \pi$ and C-H$\cdots \pi$ interactions of the incoming guest molecules with the host framework. This implies that the surface area of the guest molecule plays a major role in modulating the dynamic motion of the framework. A recent study by Bourne and co-workers revealed that a 2D MOF assembled from 34pba ligand and Zn(II) [ Zn(34pba)$_2$]$_n$ with an **sql** topology absorbed a wide range of alcohols associated with an increase in the unit cell volume.[43] The volumetric amplitude increased with an increase in the size of the alcohol. However, the MOF showed a decrease in the breathing amplitude for alcohols with more than five carbon atoms in the chain. The absorption of alcohols with diameters greater than the pores of the MOF was attributed to the $\pi \cdots \pi$ and C-H$\cdots \pi$ interactions which triggers the motion of the 2D network thereby allowing for the entry of the guest molecules. Furthermore, it has been reported that rotational linker movement causes the expansion of the pore windows and the adsorption of molecules larger than expected. In our studies[43], we concluded that the mechanism of breathing arose from rotation of the phenyl and pyridyl rings about the C-C bond which gave rise to the cleavage of the Zn-O bond resulting in the lengthening of the bend bridging ligand. Crystallographic studies revealed that the ligand adopted different conformations in the activated phase and the alcohol inclusion compounds. These ligand conformations were modulated by the size of the alcohol in the cavities. Figure 2 illustrates the change in the unit cell parameters of [Zn(34pba)$_2$]$_n$ with increase in the size of the alcohol in the cavities.
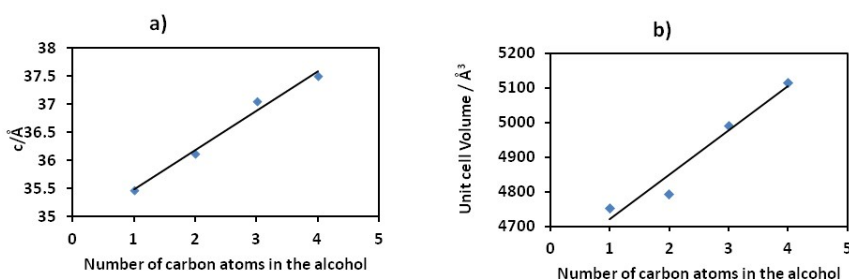


**Fig 2:** An illustration of the change in lattice parameters of the [Zn(34pba)$_2$] network with increase in the length of the carbon chain

The amplitude of breathing exhibited by the 2D MOF is far below other reported 3D MOFs[44-46]; however competition studies revealed that this material may be suitable in achieving separation of linear chain alcohols. The mechanism of the separation was based on the extent of interactions of the alcohols with the framework which initiates the dynamic motion of the 2D network allowing for the entry of the molecules. In the majority of robust metal organic frameworks studied to date the size of the pores of the framework plays a large role in achieving separation of mixed components,[47] a process similar to the familiar "molecular sieving".

### 4.0 Magnetic properties

The search for molecular magnetic materials has been of topical interest for decades with the aim of elucidating the fundamental magnetic phenomena and constructing new magnetic materials with potential applications. Coordination chemistry in particular is the most powerful tool to access such systems. Approaches such as using short bridging groups have been proposed to connect paramagnetic metal centres and to transmit magnetic coupling.[34] In this context, carboxylates have rich coordination chemistry and magenetochemistry and are capable of linking metal ions in various coordination

modes and can transmit magnetic exchange of different nature and magnitude. Because of the presence of the carboxylate moiety in 34pba and 44pba, MOFs assembled from these linkers and other auxiliary linkers have been reported to show interesting magnetic properties.

### 4.1 Magnetic properties of MOF of 34pba ligand

A helical cobalt MOF LAF-1,[26] [ $Co_2(OH)(3,4\text{-}PBC)_3$] (where 3,4-PBC is 3-(4-pyridyl) benzoate) has been reported to show significant overall antiferromagnetic properties. LAF-1 is constructed by $Co_4(II)(\mu_3\text{-}OH)$ clusters linked by the unsymmetrical 34pba ligand forming a helical double layered MOF. The magnetic susceptibility of LAF-1 which was performed at 0.1T within a temperature range of 2-350K. The value of product $\chi_m T$ at room temperature (11.7 emu·K·mol$^{-1}$) was found to be higher than the expected value of 10.8 11.7 emu·K·mol$^{-1}$ for four noninteracting Co(II) centres. The $\chi_m T$ value decreased with cooling reaching a value of 0.712 emu·K·mol$^{-1}$ at 2K. The authors suggested that these results indicate a strong antiferromagnetic coupling.

### 4.2 Magnetic properties of MOFs based on 44pba linker and other auxiliary organic ligands

A pillared layer MOF with a **bcu** topology [$Co_3(pybz)_2(pico)_2]_n$ ( pybz = 4-(pyridin-4-yl)benzoate, pico = 3-hydroxypicolinate), exhibiting a ferromagnetic long range order was assembled from cobalt(II) and a mixed ligand system.[32] The bulk magnetic behaviour of [$Co_3(pybz)_2(pico)_2]_n$ exhibits ferrimagnetic long-range ordering below 2.6 K, which mainly arises from the cooperative magnetic effect of the intra- and intertrimer arrangements in the 2D magnetic system based on the nature of the exchange mode of the hydroxyl and the bridging carboxylate moieties. Zeng *et al* [29] assembled a double-walled porous MOF , [$Co^{II}_3(lac)_2(pybz)_2]\cdot3DMF$ (**1**·3DMF, purple, where pybz = 4-pyridyl benzoate, lac = d- and l-lactate) and its post-synthetic modified (PSM) congeners, [$Co^{II}_3(lac)_2(pybz)_2]\cdot xGuest$ (*x*Guest = 6MeOH, purple; 4.5EtOH, purple; 3PrOH, purple; 2C$_6$H$_6$, purple; 2.7I$_2$, black), [$Co^{II}_3(lac)_2(pybz)_2]$ (**1**, purple), [$Co^{II}_3(pybz)_2(lac)_2(H_2O)_2]\cdot7H_2O$ (**1a**·7H$_2$O, green), and [$Co^{III}Co^{II}_2(pybz)_2(lac)_2(H_2O)_2]I\cdot2H_2O\cdot1.5DMSO$ (**1b**·I$^-$·2H$_2$O·1.5DMSO, yellow, DMSO = dimethyl sulfoxide) illustrated in Scheme 1.
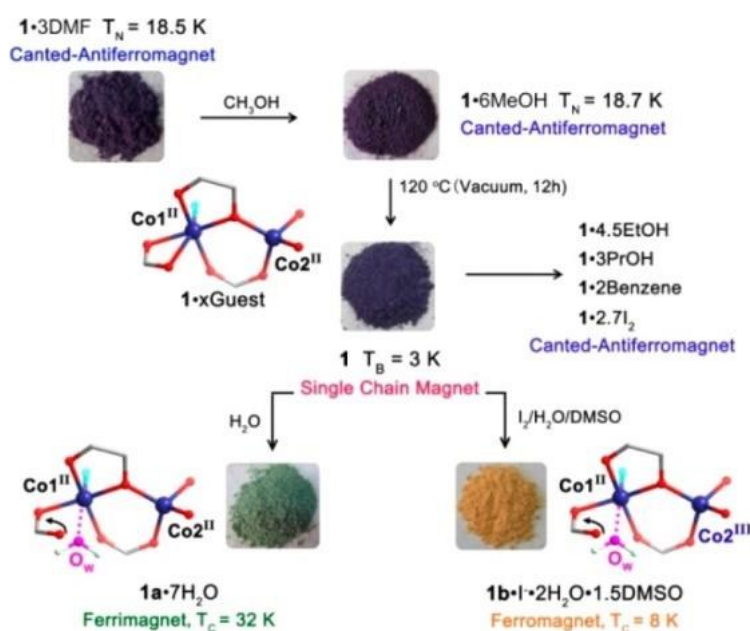


**Scheme 1:** The post-synthetic modifications and resulting magnetic ground states and changes in coordination and valence of cobalt ions. Reprinted with permission from ref 29. Copyright (2014) American Chemical Society.

Upon PSM, the magnetism is transformed from a canted antiferromagnet (**1**·3DMF and **1**·*x*Guest) to single-chain magnet (**1**), to a ferrimagnet (**1a**·7H$_2$O), and to a ferromagnet (**1b**·I$^-$·2H$_2$O·1.5DMSO) as illustrated in Figure 3. This magnetic transformation was explained on the basis of different interchain exchanges ($J'$), antiferromagnetic for **1**·3DMF and **1**·*x*Solvent ($J' < 0$), SCM for **1** ($J'$ verge to 0), and ferromagnetic for **1a**·7H$_2$O ($J' > 0$), between homometal topological ferrimagnetic chains (two octahedral and one tetrahedral Co$^{II}$ ions) connected by the double walls of pybz at 13.3 Å (shortest

Co···Co). For **1b·I⁻·2H₂O·1.5DMSO** the moment of the tetrahedral site is turned off, thus stabilizing a ferromagnetic state ($J' > 0$). The present stabilization of four magnetic ground states has not yet been observed in MOFs.
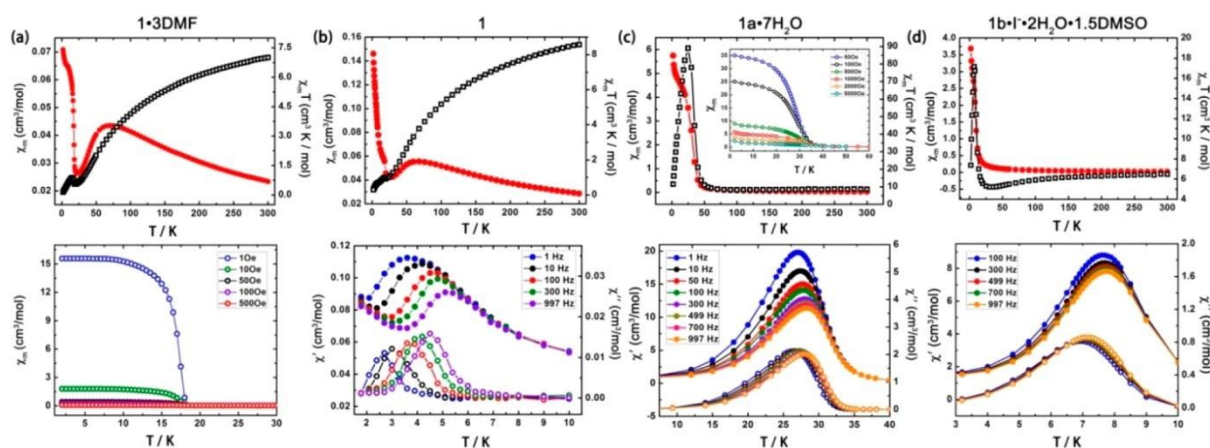


**Fig 3:** The temperature dependence of the dc and ac magnetic susceptibilities of four different magnetic ground states. Reprinted with permission from (ref 29). Copyright (2014) American Chemical Society.

Two MOFs of Mn and Cu were syntheised using 44pba and NaN₃ comprising of azide and/or carboxylate bridges.[34] The Cu-MOF {[Cu ₂(44pba)₃(N₃)]·3H₂O}ₙ, consists of 2-fold interpenetrated 3D coordination networks with the α-**Po** topology, in which the six-connected dinuclear motifs with mixed (μ-EON₃)(μ-COO)₂ (EO = end-on) triple bridges are linked by the 44pba spacers. The Mn-MOF [Mn(44pba)(N₃)(H₂O)₂]ₙ,contains 2D Mn(II) coordination networks in which the chains with single μ-EE-N₃ (EE = end-to-end) bridges are interlinked by the 44pba ligands. The structure also comprises of a 2D hydrogen-bonded network in which Mn(II) ions are linked by double triatomic bridges,(μ-EE-N₃)(O-H…N)and(O-H…O)₂. Magnetic studies on the Cu-MOF indicated that the mixed azide and carboxylate bridges induce ferromagnetic coupling between the Cu(II) ions while the Mn-MOF features antiferromagetic coupling through the EE azide bridges. Figure 4 illustrates the structural features of the two MOFs and the magnetic susceptiblity data.
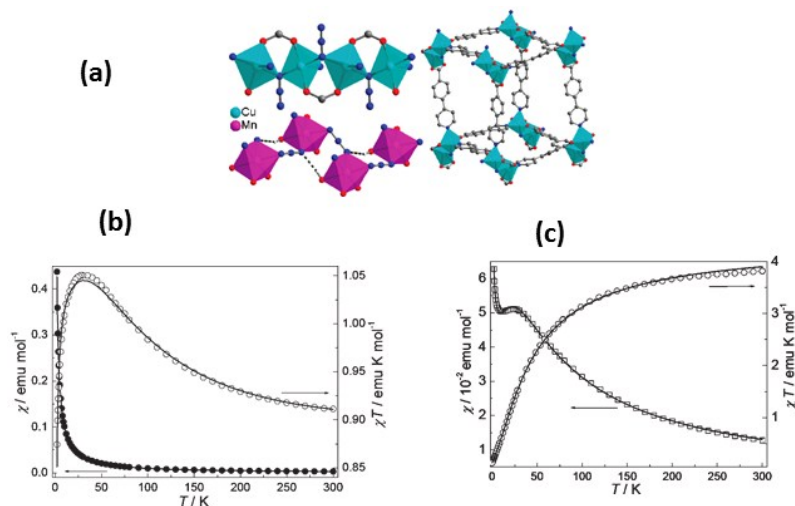


**Fig 4** : (a) Structural features of the Cu-MOF and Mn-MOF, (b) Temperature dependence of χ and χT for the Cu-MOF under 1kOe, (c) Temperature dependence of χ and χT for the Mn-MOF under 1kOe. The solid lines represents the best fit to the Fisher model; Reprinted with permission from (ref 34). Copyright (2014) American Chemical Society.

**5.0 Luminescence behaviour**

The development of MOFs has offered a unique platform for the design of solid-state luminescent materials as they have a degree of structural predictability. The inherent porosity in MOFs leads to luminescent features that have not yet been observed for traditional inorganic complexes. The ability of MOFs to absorb guest molecules into the pores allows the species to be immobilised in close proximity with the luminescent centres. The emission behaviour may be affected by the presence of the guest, which leads to wavelengths shifts, intensity change or even formation of new emission as a result of excimer or exciplex formation. Luminescence in MOFs may arise from different mechanisms which are (a) the organic linker, in this instance conjugated organic linkers which absorb in the UV and visible region. (This emission can be from the linker or can involve a metal to ligand charge transfer) (b) framework transition metal ion with unpaired electrons can be efficient quenchers. (Lanthanides have also been reported to emit sharp luminescence from forbidden transitions,) and (c) the interaction of guest lumophores with the framework may result in emissive properties in an otherwise non-emissive material.

### 5.1 Luminescence of MOFs based on 34pba linker

Networks assembled using 34pba and 44pba linkers have also demonstrated luminescence behaviour. Wei-Hou and co-workers reported a series of networks $[Ni(L)_2(C_2H_6O_2)]_n$ , $\{[Cd(L)_2(H_2O)_2]\cdot 4H_2O\}_n$ , $[Zn_2(OH)(L)_3]_n$ , $[Fe_2(OH)(L)_3]_n$ , $[Ni(L)_2(H_2O)]_n$ and $[Cd(L)_2(H_2O)]_n$ where L is 34pba exhibiting photoluminescence properties.[24] These compounds have abounding structure chemistry ranging from one-dimensional ribbons ($[Ni(L)_2(C_2H_6O_2)]_n$ and $[Cd(L)_2(H_2O)_2]_n\cdot 4H_2O$), and two-dimensional novel helical double-layered frameworks ($[Zn_2(OH)(L)_3]$ and $[Fe_2(OH)(L)_3]_n$) to three-dimensional CdSO$_4$-topological porous interpenetrating architectures with hydrophilic and hydrophobic channels regularly arraying ($[Ni(L)_2(H_2O)]_n$ and $[Cd(L)_2(H_2O)]_n$). The photoluminescence was found to have different intensities owing to structural diversity and coordinated water molecules. This luminescence was ascribed to a ligand-centred $\pi$ to $\pi^*$ excitation. Niu *et al* reported five coordination networks of 34pba and Zn(II), which were synthesised in the presence of dicarboxylic acids and nitrolotriacetic acid as secondary ligands to tune the coordination mode of the 34pba ligand.[48] These compounds exhibited strong fluorescent emissions at room temperature. The fluorescence behaviour was ascribed to the metal perturbed intraligand emission state just like other d$^{10}$ metal complexes and other intermolecular interactions such as $\pi-\pi$ packing lying in interpenetration, interdigitation, or simple packing of layers. Their fluorescence behaviour indicates that they are good candidates for potential photoactive materials.

### 5.2 Luminescence of MOFs based on 44pba linker

Yang and co-workers fabricated the first two three-fold interpenetrated frameworks, $[LnCuL_4][Ln_{0.25}Cu_{0.25}L]$ (Ln = Dy **1**, Er **2**; HL = 4-(pyridin-4-yl)benzoic acid). [28] The structures contain two kinds of four-connected uniform nets: **dia** and **mdf** nets which are interpenetrated (see Figure 5). The luminescence properties of these compounds were studied at room temperature in the solid state. The two compounds showed broad fluorescent emission spectra from 500 to 700 nm which were attributed to metal to ligand charge transfer.[31]
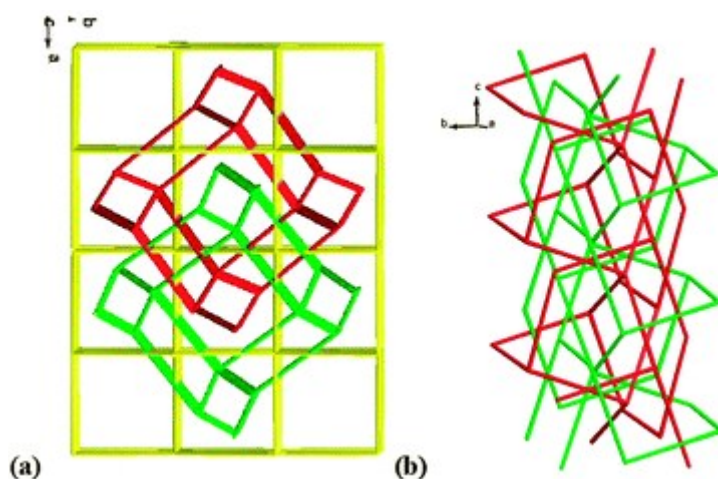


Fig 5: Three-fold interpenetration between two **mdf** nets and one **dia** net.

### 6.0 Thermal expansion properties

Mechanoresponsive MOFs hold great technological potential in drug delivery, smart optical systems and microelectromechanical system. One particular interesting property of MOFs is the ability to undergo thermal contraction upon application of heat. This has been attributed to energy transverse vibrations of molecular bridges within the open framework structures.[11] By tuning the energy of the vibrational modes, large negative thermal expansion (NTE) and approximate zero expansion has been achieved in MOFs. Recent studies have highlighted an unusual mechanism of NTE in MOFs which is based on interpenetration.[49] NTE expansion has been linked to structural changes the framework undergoes when exposed to heat. Some interpenetrated MOFs glide upon application of heat resulting in the reduction of the total volume, the amplitude which increases with increase in temperature.

Scheme 2 illustrates the structures and topologies of some of the MOFs assembled from pyridylbenzoates ligands which exhibit interesting thermoresponsive properties
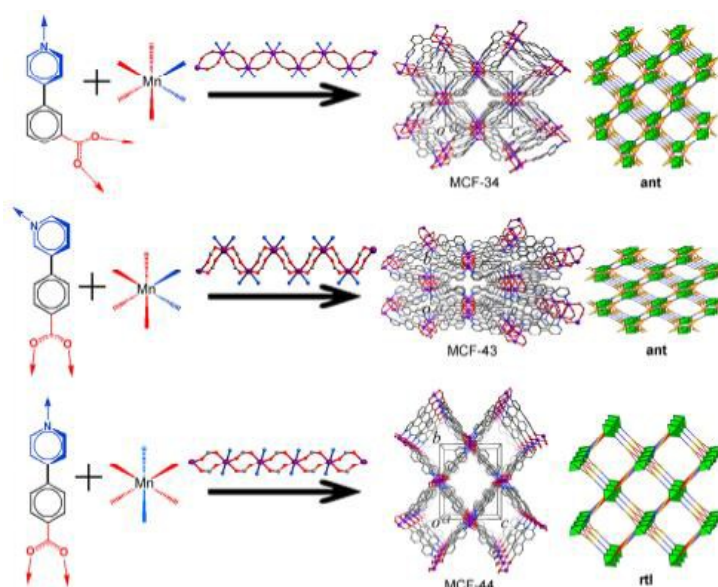


**Scheme 2**: Self-assembly, structures and topologies of MCF-34, MCF-43, and MCF-44 from $Mn^{2+}$ ions and pyridylbenzote ligands. With kind permission from Springer Science and Business Media.

### 6.1 Thermal expansion of MOFs of 34pba linker

MCF-34, $[Mn(34pba)_2]_n$ assembled from 34pba and Mn(II) under solvothermal conditions exhibited huge NTE and PTE properties. In MCF-34 the ligand 34pba exhibits a low rotational barrier energy between the pyridyl and phenyl ring which serves as a tripodal node to connect the octahedral Mn(II) ions to construct an ultramicroporous network bearing a 3,6-conneceted **ant** network. MCF-34 exhibits large PTE ($\alpha = +224 \times 10^{-6} K^{-1}$) and a NTE ($\alpha = -107 \times 10^{-6} K^{-1}$). Crystallographic studies revealed that the decrease in the N-Mn-N angle caused lengthening of the *b*-axis significantly and shortening of the *c*-axis by a small magnitude was responsible for the thermal expansion behaviour observed. The thermal expansion properties for MCF-34 were reported to be exceptional because their coefficients are among the largest values known for MOFs and were constant in the widest temperature range even in open conditions. The guest responsive thermal properties of MCF-34 were also evaluated. The studies revealed unique reversible thermal expansion behaviour of crystals loaded with DMF and DMA molecules in the ultramicropores. Table 2 gives the thermal expansion properties of MCF-34 and other representative MOFs under different conditions. The reversible thermal expansion behaviour was studied over a narrow temperature range and was attributed to the expansion of the guest or guest relocation within the ultramicropores. Kepert and coworkers reported isotropic PTE of $+10.0 \times 10^{-6} K^{-1}$ and a negative thermal expansion of $-33.5 \times 10^{-6} K^{-1}$ upon guest removal in $Cd(CN)_2 \cdot xCCl_4$. In a related study Babour's group showed that the PTE of Zn(OH)(niba)]·alcohol can be increased by $90 \times 10^{-6} K^{-1}$ upon changing the alcohol guest molecules.[50]

### 6.2 Thermal expansion of networks of 44pba linker

$\{[Mn(44pba)_2]\cdot2.5DMF\}_n$ (MCF-44) constructed from 44pba and Mn(II) had NTE($\alpha$ = -148 x $10^{-6}$ K$^{-1}$)/ PTE($\alpha$ = +381 x $10^{-6}$ K$^{-1}$) coefficients greater than those of MCF-34.[18] The framework of MCF-44 has an **rtl** topology. The thermal expansion behaviour of MCF-44 was attributed to the changes in the dihedral angles between the pyridyl and phenyl ring as well as its large pore volume. Zhou *et al* constructed a MOF comprising of the bend ligand 34pba and the linear ligand 44pba with Cd(II) ions $[Cd(34pba)(44pba)]_n$, MCF-82.[27] Their reaction gave rise to a 3D hinge-like structure with multimode flexibility but also quasi-0D ultramicropores suitable for adsorption and confinement of pairs of different amide-type guests. Figure 6 depicts the structural features and the **bcu** topology of MCF-82.
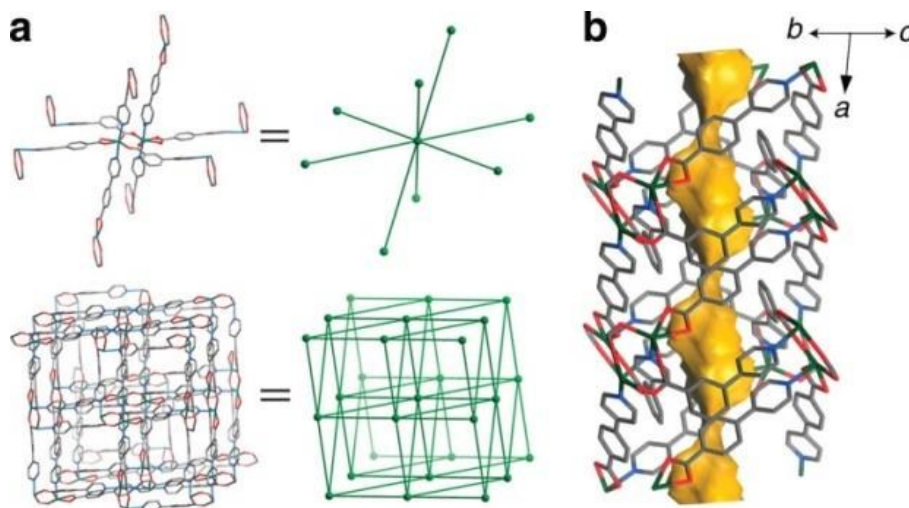


**Fig 6:** (**a**) View of 3D coordination framework of MCF-82 along the *a*-axis the corresponding network topology (the aromatic rings of the 34pba and 44pba ligands are highlighted in blue and yellow, respectively), (**b**) Cavities found in MCF-82 as viewed along the [011] direction. Reprinted by permission from Macmillan Publishers Ltd: [Nature] (reference citation 27), copyright (2015).

Single crystal X-ray diffraction studies under different temperatures of MCF-82 and guest stimuli revealed unprecedented negative thermal expansion and positive thermal expansion reported to date as illustrated in Figure 7.
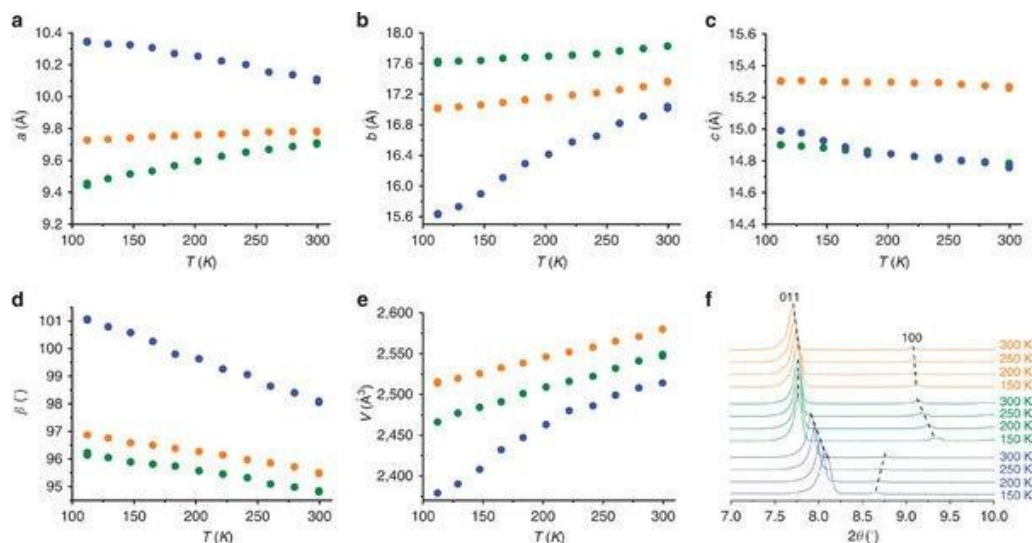


**Fig 7**: a-e, temperature induced unit cell parameters of MCF-82 (blue) , MCF-82·DMF (green), MCF-82·DMA determined by single crystal X-ray diffraction, (f) PXRD patterns of MCF-82 (blue) , MCF-82·DMF (green), MCF-82·DMA (orange). Reprinted by permission from Macmillan Publishers Ltd: [NATURE] (reference citation 27), copyright (2015).

Temperature dependent PXRD studies of the MCF-82 revealed giant PTE ($\alpha$ = 482 x $10^{-6}$ $K^{-1}$) and NTE ($\alpha$ = -218(3) x $10^{-6}$ $K^{-1}$) along the *b* and *c*-axes respectively. The authors noted that the PTE and NTE of MCF-82 are very large in comparison to other reported crystalline materials. They concluded that these thermoresponsive properties arise from variation of the coordination angles rather than the coordination bonds. They further argued that despite the high symmetry endowed by the framework, which allows deformation to take place from any direction the real deformation manner depends on the anisotropy of the coordination network and pore system, as well as the distribution of the guest molecules. MCF-82 can absorb/release DMF and DMA vapour at room temperature to give MCF-82: DMF and MCF-82:DMA respectively which are isomorphic with MCF-82 in a single crystal to single crystal manner. The unit cell parameters of the guest loaded crystals change linearly against temperature. MCF-82: DMF crystals exhibited a huge PTE along the *a*-axis ($\alpha$ =171 x $10^{-6}$ $K^{-1}$) with moderate PTE ($\alpha$ = 60 x $10^{-6}$ $K^{-1}$) and NTE ($\alpha$ = -56 x $10^{-6}$ $K^{-1}$) along the *b* and *c*-axes respectively. It was noted that when DMF was replaced with DMA, the thermal expansion coefficients along the *a*-axis was halved while that along the *b*-axis doubled with the *c*-axis remaining almost constant. The work by Zhou *et al* clearly demonstrates the guest-modulation effect on the PTE and NTE properties of MCF-82. Table 2 summarises the thermal expansion properties of the pyridylbenzoate MOFs and some representative materials.

Table 2: Axial thermal expansion coefficients of MOFs made using the 44pba and 34pba linkers and some representative materials reported to have high thermal expansion coefficients.

| Name of MOF | $\alpha$/PTE x $10^{-6}$ $K^{-1}$ | $\alpha$/NTE x $10^{-6}$ $K^{-1}$ | Ref |
|---|---|---|---|
| MCF-34 | +224 (1) | -107 (1) | [19] |
| MCF-34: DMA | +213 (5) | -101 (2) | [19] |
| MCF-34 : DMF | +152 (3) | -56 (5) | [19] |
| MCF-34: DMF | +237 (6) | -116 (5) | [19] |
| MCF-44 | +381 | -148 | [18] |
| MCF-82 | +482 | -218 | [27] |
| MCF-82DMF | +171 | -56 | [27] |
| MCF-18.DMF | +437 | | [46] |
| MCF-18.MeOH | +242 | | [47] |
| MCF-18 | +81 | | [47] |
| FMOF-1 | +230 | -170 | [51] |
| HMOF-1 | +177 | | [52] |
| [Zn(OH)(niba)] | +137 | | [50] |
| [Zn(OH)(niba)·MeOH] | +166 | | [50] |

### 7.0 Exceptional iodine Capture

The development of porous materials is exceedingly topical and specific attention has been directed at crystalline materials capable of capturing iodine.[53-55] Such materials are gaining momentum because of the particular properties of iodine such as conductivity and polarity. The increase in use of nuclear energy to meet human demands, waste management from nuclear plants has become more important than before. The main risks associated with nuclear waste include health effects of radiation which may lead to cancer. Iodine-129 ($^{129}$I), an important radionuclide in nuclear waste, has a very long half-life of 15.7 million years and has hence generated special interest and concern. However, the efficient capture and reliable storage of radioactive gaseous iodine $I_2(g)$ in nuclear effluents remains a big challenge. Silver-based zeolites adsorbents are currently used in the capture of radioactive $I_2(g)$. These silver loaded adsorbents have high loading capacity and removal efficiency; however, they have key disadvantages such as high cost and the adverse environmental impact of silver.

**7.1 Iodine Capture by MOFs of 44pba linkers**

MOFs assembled from 44pba linkers revealed high levels of iodine capture. This is because the 44pba ligand allows for maximum interactions of the iodine in the cavities with the aromatic framework. One particular example is a MOF assembled from zinc(II) and 4-(4-pyridyl)benzoate $\{[Zn_3(dl\text{-}lac)_2(pybz)_2]\cdot 3DMF\}_n$ (dl-**lac**=lactate, pybz=4-(4-pyridyl) benzoate) whose structural features are displayed in Figure 8. The activated phase showed some interesting iodine uptake of 1.01g/g [4] exceeding those of zeolite 13X (0.32-0.38 g/g), activated carbon (0.84g/g) and other systems.[15,53-58] It was concluded that the high uptake of iodine was attributed to attributed to the structural character from the regular π-electron walls comprised of 4-(4-pyridyl)benzoate ligands.
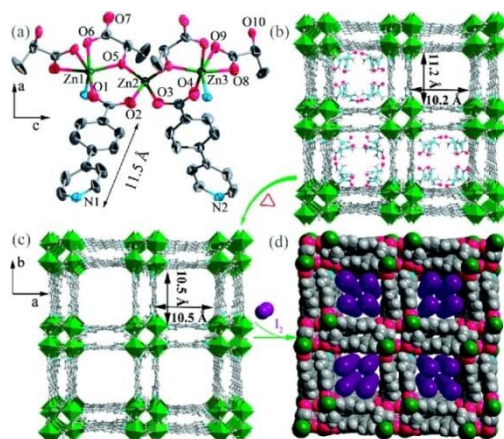


**Fig 8:** A schematic illustration of the double walled MOF by Zeng *et al* [4] (a) coordination environment of the zinc (II) ions, (b) the crystal structure of the MOF with guest molecules in the channels, (c) the empty framework highlighting the sizes of the channels (d) the expected structure of the iodine loaded compound. Reprinted with permission from (ref 4). Copyright (2010) American Chemical Society

In contrast to the Zn(II) analogue the Co(II) compound absorbed 0.9 g/g of iodine from cyclohexane solution and was oxidized in the process.[33] The release of iodine from the two isostructural compounds was studied in ethanol which revealed that the two system released iodine at a slow rate. The slow release of iodine was attributed to the strong interaction of the iodine molecules with aromatic walls of the MOFs. Inspired by Zeng and co-workers Mehlana evaluated the uptake of iodine using a diamondoid network assembled from 44pba and Ni(II), [Ni(44pba)] under solvothermal conditions. The empty network exhibited high levels of iodine uptake of 1.1g/g when exposed to iodine vapour for 14 days.[59] The greater iodine uptake achieved was attributed to the 47 % free channel volume compared to the 43.5 % found in the double-walled MOF. A comparison of the iodine uptake by 44pba MOFs with other MOFs reported in literature is presented in Table 3.

Table 3: Lists of 44pba MOFs with high iodine capture and a representative of non- 44pba MOFs that have shown considerable iodine capture.

| Formula of MOF | % weight of $I_2$ | Ref |
|---|---|---|
| [a]$\{[Ni(44pba)]\cdot 2I_2\}_n$ | 51.1 | [59] |
| [a]$\{[Zn_3(dl\text{-}lac)_2(44pba)_2]\}_n$ | 49.7 | [4] |
| [a]$\{[Co_3(dl\text{-}lac)_2(44pba)_2]\}_n$ | 47.7 | [33] |
| $\{[Zn(C_5H_5N_2O_2)]\cdot 2.2I_2\}_n$ (ZIF-1) | 63.9 | [60] |
| $\{[Ni_2(C_{26}H_{52}N_{10})]_3[BTC]_4\cdot 6C_5H_5N\cdot(I_3)4\cdot 5I_2\cdot 17H_2O\}_n$ | 48.2 | [61] |
| $\{[Cu_2(bitmb)_2Cl_4]\cdot I_2\}_n$ | 23.4 | [62] |
| $\{[Zn(C_6H_8O_8)]\cdot 0.5H_2O\cdot 0.3I_2\}_n$ | 21.2 | [63] |
| $[Zn_7(L1)_3]_n\cdot[Zn_5(L1)_3]_n$ | 13.9 | [64] |
| [a]$\{[Cu_6(pybz)_8(OH)_2]\cdot I_5\cdot I_7\}_n$ | 43.2 | [15] |
| $\{[(Me_2NH_2)_2]\cdot[Cd_3(5\text{-}tbip)_4]\cdot 4.2I_2\}_n$ | 36.7 | [65] |

[a]Represents MOFs assembled using the 44pba ligand discussed in this review. DL-lac = DL-lactate; Na3BTC = 1,3,5-benzenetricarboxylate; bitmb =1,3-bis(imidazol-1-ylmethyl)-2,4,6-trimethylbenzene; L1 = N-phenyl-N0-phenylbicyclo[2,2,2]oct-7-ene-2,3,5,6-tetracarboxdiimide tetracarboxylic acid, 5-tbip =5-tbipH2: 5-tert-butylisophthalic acid

## 8.0 Vapochromic/solvatochromic and thermochromic behaviour

Vapochromic/solvatochromic and thermochromic behaviour are fundamental properties that can be exploited for sensing. Solvatochromism is the change in colour upon absorption of a solvent molecule into the channels of a MOF while thermochromism is the change in the absorption spectra of a compound upon heating. Several studies have suggested that the chromic effects in MOFs arises from metal to ligand charge transfer[66], change in the crystal packing of the compound which affect the HOMO and LUMO energy levels, disruption of the supramolecular interactions which in turn trigger the $\pi$-$\pi$* transitions and loss of coordinated solvent molecules around the metal centre which affects the crystal field energy splitting.[67-69] The change in the binding mode of the carboxylate moiety has been reported to have an effect on the chromic properties of MOFs.[12]

## 8.1 Solvatochromism and vapochromism in 44pba MOFs

Zeng *et al* and Mehlana *et al* reported a 2+2 fold **dia** network assembled from 44pba and Co(II) under solvothermal conditions[29,30] which exhibited thermochromic and solvatochromic behaviour. Zeng *et al* reported the MOF as $\{[Co(II)(pybz)_2]\cdot 2DMF\}_n$ [pybz = 4-(4-pyridyl)benzoate] crystallizing in a chiral space group P42$_1$2 while Mehlana *et al* reported it as $\{[Co_4(44pba)_8]\cdot 3DMF\cdot 0.25EtOH\cdot 4H_2O\}_n$ with a different space group of *I4*. The difference in the amount of the guest molecules occupying the channels in this compound can be attributed to the different solvent systems that were used during synthesis. $\{[Co(II)(pybz)_2]\cdot 2DMF\}_n$ was synthesised using DMF while $\{[Co_4(44pba)_8]\cdot 3DMF\cdot 0.25EtOH\cdot 4H_2O\}_n$ was synthesised using a solvent mixture of DMF/ethanol in the ratio of 5:2 respectively. Figure 9 shows the structural features of $\{[Co(II)(pybz)_2]\cdot 2DMF\}_n$.
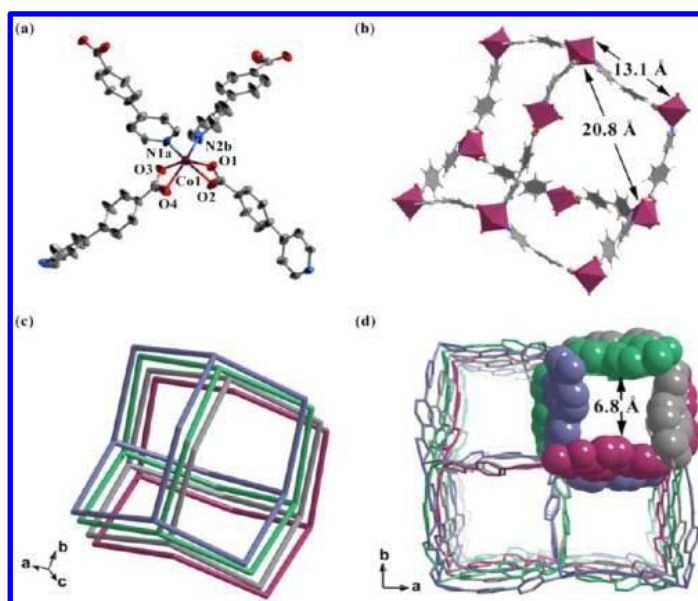


**Fig 9** (a) Coordination geometry of the Co(II), (b) a single diamondoid network found in the porous network (c) topological representation of the four-fold diamondoid network, (d) channels found in the network running along the [001] direction. Reprinted with permission from (ref 29). Copyright (2013) American Chemical Society.

Both groups reported that when single crystals of the synthesised material are exposed to air, the purple crystals changed colour from purple to yellow accompanied by a significant loss in crystallinity (Figure 10). Interestingly when the yellow crystals are heated the purple colour is restored. The compounds could be activated without loss in crystallinity. Upon exposure of the activated phase to various solvent molecules, the framework displayed different colours depending on the nature of the solvent absorbed into the channels. These colour changes were attributed to the change in the crystal packing of the network induced by hydrogen bonding interactions between the solvent molecules and the host framework and metal to

ligand charge transfer transitions. Solid state UV-Vis studies revealed that the colours observed were consistent with the absorption spectra of the inclusion compounds. The authors concluded that the material can be used for sensing water and other small molecules.
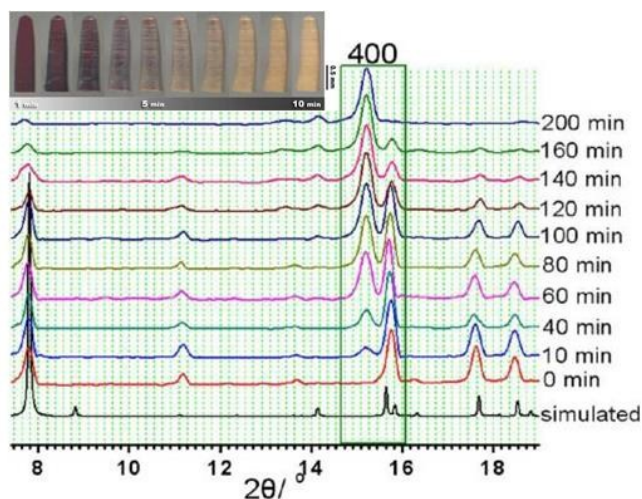


**Fig 10:** Time dependent PXRD of Co(II)(pybz)$_2$·2DMF in air at room temperature: Insert, crystals of Co(II)(pybz)2·2DMF undergoing a colour change from purple to yellow at 65% humidity . The same phenomenon was also reported earlier on by Bourne and co-workers. Reprinted with permission from (ref 29). Copyright (2013) American Chemical Society.

Bourne and co-workers studied the structural transformations of {[Co$_4$(44pba)$_8$]·3DMF·0.25EtOH·4H$_2$O}$_n$ mediated by soaking the crystals in dry methanol for four weeks (Figure 11).[31] The **dia** network transformed to a **quarzt** net via the intermediate **pts** net. The **quarzt** net could be transformed back to the **dia** network by soaking the compound in DMF for several hours. The reversibility of the network was ascribed to topology information transfer from the guest network to the framework. The solvatochromic effects observed during these transformations were due to the coordination of the methanol molecules to the Co(II) and change in the coordination mode of the carboxylate group from bidentate to mono-dentate.
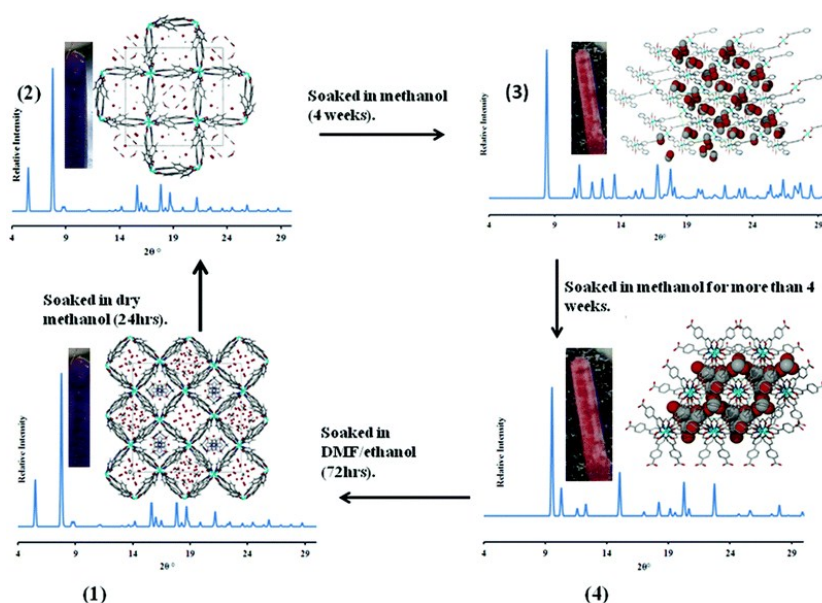


**Fig 11**: An illustration of the structural transformations {[Co$_4$(44pba)$_8$]·3DMF·0.25EtOH·4H$_2$O}$_n$ (1) to give a **pts** net (3) and a **quarzt** net (4). These transformations are accompanied by visible colour changes.[31]

Literature documents several MOFs exhibiting solvatochromic properties; however none of these MOFs are as sensitive to moisture or water as the 44pba MOFs. [70,71] Zhong Lu *et al* used a solvatochromic ligand 3,6-di(pyridine-4-nl)-1,2,4,5-tetrazine (dptz) and Cu (I) was chosen as the metal centre since it has a d10 configuration and therefore allows one to observe low lining electronic transitions. The reaction of the chosen components gave a nanotubular MOF $\{[(WS_4Cu_4)I_2(dptz)_3]\bullet DMF\}_n$ (dptz = 3,6-di(pyridin-4-yl)-1,2,4,5-tetrazine, DMF = N,N-dimethylformamide). The nanotubular compound exhibited reversible solvatochromic response upon inclusion of different solvent guests ($CH_3CN$, $H_2O$, $CH_3OH$, DMF, Acetone, $C_2H_5OH$ and $CHCl_2$) in its channels which was easily noticed by visual colour change. The solvatochromic behaviour of the nanotubular MOF was attributed to MLCT. It was also noted that the ligand used for synthesis played a major role in the solvatochromic response of the MOF, which was ascribed to the strong π- acceptor property as well as the liable electronic structure to the solvent polarity.[72] Encouraged by the findings of Zhong Lu *et al* , Sun *et al* [71] evaluated the solvatochromic effects of a mesoporous chiral MOF assembled from a predesigned hexatopic ligand 5, 5', "-(1,3,5,-triazine-2,4,6-triyl) tris-(azanediyl) triisophthalate (TATAT) and zinc (II) ions. The solvothermal reaction product obtained was a 3D anionic MOF. Unlike the 44pba MOFs which show dramatic colour changes when exposed to solvent vapours or immersed in solvents, samples of the 3D chiral network immersed in acetone and ethanol, showed a visible colour change from colourless to light yellow after 30 minutes.

### 8.2 Thermochromism in coordination networks of 34pba and Co(II)

Bourne and co-workers fabricated two molecular building blocks structural isomers with the same elemental composition having a molecular formula $[Co(34pba)_2\cdot DMF]_n$.[12] . The large crystal in Figure 12 has an 8-connected **bcu** net while the small crystal has an **sql** net. As illustrated in Figure 12, the crystals changed from pink to deep blue upon heating. This phenomenon was studied by IR and variable temperature PXRD. The mechanism of the thermochromic behaviour originated from loss of the DMF molecules in the cavities which gave rise to minor modifications in the network as well as change in the binding mode of the carboxylate moiety above the phase transition temperatures.
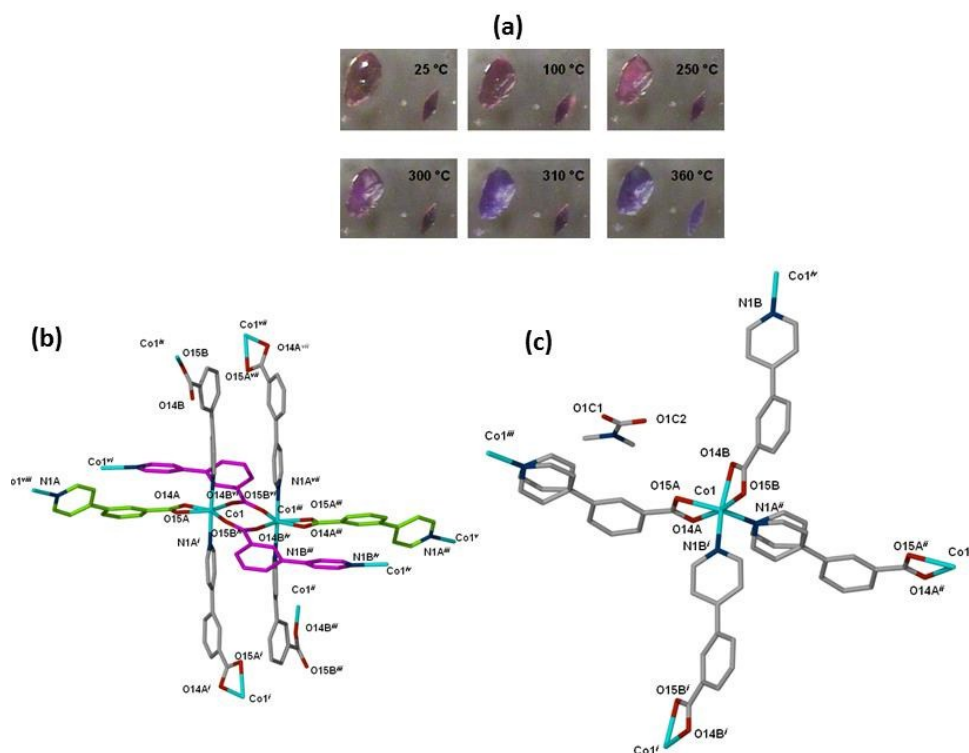


**Fig 12**: (a) Crystals of the two molecular building blocks structural isomers undergoing some colour change with heating, (b) Coordination environment of Co(II) the **bcu** net of $\{[Co(34pba)_2]\cdot DMF\}_n$ , (c) Coordination environment of Co(II) the **sql** net of $\{[Co(34pba)_2]\cdot DMF\}_n$.

Recently Mehlana *et al* evaluated the thermochromic behaviour of a 3D hydrogen discrete complex of Co(II) and 34pba, $\{Co(34pba)_2\cdot(H_2O)_4\}_n$.[25] In this compound, the Co(II) metal centre is coordinated to two nitrogen atoms from two 34pba linkers and four oxygen atoms of the four coordinated water molecules to furnish a distorted octahedral geometry. Four water molecules and two 34pba ligands bound to the metal constitute a discrete compound. These discrete units are hydrogen

bonded via the water molecules and the oxygen atoms of the carboxylate groups to form a 3D hydrogen-bonded network. The crystals of this compound changed from yellow to dark pink and finally turning blue (Figure 13).
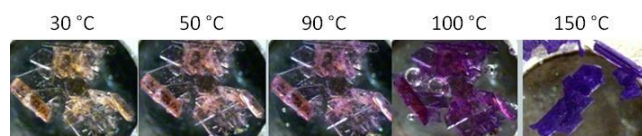


**Fig: 13**: Crystals undergoing a colour change from yellow to dark pink and finally turning blue. Reprinted from ref 25, Copyright (2015), with permission from Elsevier.
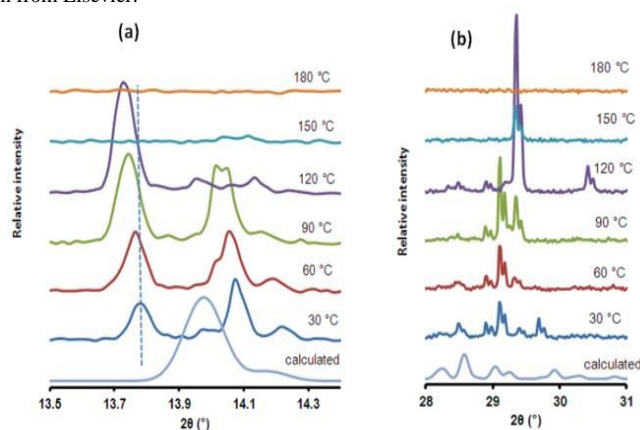


**Fig 14:** (a) Temperature dependent of the 002 reflections, (b) formation of a metastable phase before the compound becomes amorphous. Reprinted from ref 25, Copyright (2015), with permission from Elsevier.

PXRD studies in Figure 14 shows a shift in the 002 reflections with heating within a temperature range of 30 -120 °C which corresponds to expansion of the lattice parameters along the *c*-axis. Pawley fitting of the diffraction patterns at different temperatures revealed contraction of the *a*- and *b*-axes with increase in the temperature of heating. We concluded that the expansion of the lattice parameters along the *c*-axis suggests movement of the 1D layers apart which weakens the hydrogen bonding interactions between adjacent layers while the contraction of the *b*-axis enhances the intermolecular charge transfer interactions between the electron-deficient pyridyl ring and the electron rich benzoate group. We attributed the observed colour change in the temperature range of 30 – 120 °C to the disruption of the supramolecular environments or metal to ligand charge transfer transitions. There are very few articles which reports on classical thermochromism based on the disruption of the supramolecular environments. Majority of reported coordination complexes or MOFs is mainly based on change in the binding mode of the carboxylate, loss of coordinated solvent molecules, and change in the ligand conformation.[68,69] Dong and co-workers reported a MOF assembled from Cu(II) and triazole-bridged unsymmetrical ligand which showed three distinct colour changes as a result of the temperature dependent twist of the chelating ligand.[73]

**9.0 Conclusions and Perspective**

The aim of this review is to present a brief summary of the exceptional properties of MOFs assembled from 44pba and 34pba. Although these two linkers have not yet been explored extensively, the current literature documents interesting properties. These include magnetism, luminescence, solvatochromism, negative and thermal expansion of host-guest composites and breathing behaviour which has not yet been observed in other MOFs. As presented in this review the approach of using auxiliary ligands (hydroxyl, azides, 3-hydroxypicolinate and D/L-lactate) and carboxylates as co-bridges is an effective way of constructing magnetic systems. The magnetic properties of MOFs of 34pba and 44pba with other auxiliary linkers have been attributed to the rich coordination chemistry of the carboxylate moiety and the short bridging ligands which are able to connect paramagnetic metal centres and to transmit magnetic coupling. Properties such as axial NTE/PTE have been attributed mainly to the flexibility of the ligands which undergoes reversible change in conformation upon external stimuli and the change in the coordination angles around the metal centre. The work by Zhou *et al* demonstrates the importance of the combination framework flexibility and ultramicropores in MOFs as an effective way to construct unprecedented and controllable thermoresponsive materials. Furthermore, the presence of guest molecules in the

ultramicropores of MCF-34 and 82 revealed how the guest molecules modulate the thermal expansion properties of these materials.   The luminescence behaviour of MOFs constructed using the 34pba and 44pba linkers mainly arise from ligand centred transitions such as

$\pi$ to $\pi^*$. The mechanism of the colour change upon absorption of water by the framework of Co(II) and 44pba reported by Bourne and co-workers arises from molecular distortions induced by strong hydrogen bonding. The thermochromic behaviour of the networks of 34pba with Co(II) arises from change in the energy difference between the asymmetric and symmetric carboxylate stretches. Flexible hydrogen bonded networks revealed that thermochromism may also arise from the disruptions of the supramolecular environments such as hydrogen bonding and $\pi\cdots\pi$ interactions  which trigger metal to ligand charge transfer transition and $\pi$ to $\pi^*$ transitions.  The work presented in this review shows that the two linkers 34pba and 44pba can also be combined with other ligands in the construction of MOFs to obtain interesting structures with important potential applications.

The simplest linker in this family of pyridylcarboxylate compounds nicotinic acid has been used in the design and construction of a MOF for biomedical application.[74] The mechanism of this MOF was based on biodegradation to release the bioactive molecule nicotinic acid as opposed to the other MOFs in which the bioactive molecules is loaded in the pores and delivered to the target site upon degradation. The same may not be the case with the 34pba and 44pba ligands since they have acute toxicity. MOFs of 34pba and 44pba may find application is in chemical sensing.  By taking advantage of the intrinsic fluorescent properties of the 44pba and 34pba ligands, cylometalated Ir complexes can be incorporated into MOFs assembled from the pyridlybenzoate linkers which may lead to highly phosphorescent materials for chemical sensing.[75]In this regard we foresee that there may be a burgeoning field of porous MOFs for chemical sensing using pyridylcarboxylate, which should have a brilliant future and may undergo an explosive growth. The dynamic nature of pyridylbenzoate MOFs which allows them to respond to external stimuli such as heat, guest molecules and pressure. These materials may find applications designing sensitive thermomechanical actuators. Heterogeneous catalysis is an area that has received a great deal of attention recently. Due to the lack of functionality in the 34pba and 44pba linkers, there are no reports in which these materials have been applied in this field. With high porosities that are normally achieved using the 44pba linker it would be possible to integrate functional species with catalytic properties to give composite materials. These composite materials may then find applications in different areas of catalysis. For example the MOFs maybe loaded with frustrated Lewis pairs (FLP) to give a composite material which may be used in the catalytic hydrogenation of carbon dioxide to formic acid and methanol. The linkers can also be functionalised using the FLP to impart catalytic conversion of carbon dioxide through hydrogenation.
  Considering the fact the 34pba and 44pba based MOFs have shown interesting properties. A lot of work has to be devoted towards the functionalisation of these linkers to produce materials with superior properties for applications in sensing, storage and catalysis.

**Acknowledgements**

**References**

1.     J. Liu, L. Chen, H. Cui, J. Zhang, L. Zhang, and C.-Y. Su, *Chem. Soc. Rev.*, 2014, 6011.

2.     B. Chen, L. Wang, Y. Xiao, F. R. Fronczek, M. Xue, Y. Cui, and G. Qian, *Angew. Chem. Int. Ed. Engl.*, 2009, **48**, 500.

3.     M. Dincă and J. R. Long, *Angew. Chem. Int. Ed. Engl.*, 2008, **47**, 6766.

4.     M. Zeng, Q. Wang, Y. Tan, S. Hu, H. Zhao, and L. Long, *J. Am. Chem. Soc.*, 2010, **132**, 2561.

5.     S. Yang, X. Lin, W. Lewis, M. Suyetin, E. Bichoutskaia, J. E. Parker, C. C. Tang, D. R. Allan, P. J. Rizkallah, P. Hubberstey, N. R. Champness, K. M. Thomas, A. J. Blake, and M. Schröder, *Nat. Mater.*, 2012, **11**, 710.

6.     C. Zou and C.-D. Wu, *Dalton Trans.*, 2012, **41**, 3879.

7.     Q. Huang, J. Cai, H. Wu, Y. He, B. Chen, and G. Qian, *J. Mater. Chem.*, 2012, **22**, 10352.

8.     S. R. Batten, N. R. Champness, X. Chen, J. Garcia-martinez, S. Kitagawa, L. Öhrström, M. O. Keeffe, M. P. Suh, and J. Reedijk, *Pure Appl. Chem.*, 2013, **85**, 1715.

9.    H.-Y. Lin, J. Luan, X.-L. Wang, J.-W. Zhang, G.-C. Liu, and A.-X. Tian, *RSC Adv.*, 2014, **4**, 62430.

10.   O. M. Yaghi, M. O'Keeffe, N. W. Ockwig, H. K. Chae, M. Eddaoudi, and J. Kim, *Nature*, 2003, **423**, 705.

11.   N. Lock, Y. Wu, M. Christensen, L. J. Cameron, V. K. Peterson, A. J. Bridgeman, C. J. Kepert, and B. B. Iversen, *J. Phys. Chem. C*, 2010, **114**, 16181.

12.   G. Mehlana, S. A. Bourne, G. Ramon, and L. Öhrström, *Cryst. Growth Des.*, 2013, **13**, 633.

13.   J. Zhou, G. Bian, J. Dai, Y. Zhang, Q. Zhu, and W. Lu, *Inorg. Chem.*, 2006, **45**, 8486.

14.   A.-M. Stadler, N. Kyritsakas, G. Vaughan, and J.-M. Lehn, *Chemistry*, 2007, **13**, 59.

15.   Z. Yin, Q. Wang, and M. Zeng, *J. Am. Chem. Soc.*, 2012.

16.   Y.-B. Zhang, W.-X. Zhang, F.-Y. Feng, J.-P. Zhang, and X.-M. Chen, *Angew. Chem. Int. Ed. Engl.*, 2009, **48**, 5287.

17.   Y.-B. Zhang, H.-L. Zhou, R.-B. Lin, C. Zhang, J.-B. Lin, J.-P. Zhang, and X.-M. Chen, *Nat. Commun.*, 2012, **3**, 642.

18.   H. Zhou, M. Li, D. Li, J. Zhang, and X. Chen, *Sci. China Chem.*, 2014, **57**, 1.

19.   H.-L. Zhou, R.-B. Lin, C.-T. He, Y.-B. Zhang, N. Feng, Q. Wang, F. Deng, J.-P. Zhang, and X.-M. Chen, *Nat. Commun.*, 2013, **4**, 2534.

20.   O. R. Evans, W. Lin, N. Carolina, and C. Hill, *Chem Mater*, 2001, **13**, 2705.

21.   T.-B. Lu and R. L. Luck, *Inorganica Chim. Acta*, 2003, **351**, 345.

22.   G. Mehlana and S. A. Bourne, *CrystEngComm*, 2014, 8160.

23.   G. Mehlana, G. Ramon, and S. a. Bourne, *Zeitschrift für Krist. - Cryst. Mater.*, 2013, **228**, 318.

24.   B.-L. Wu, R.-Y. Wang, H.-Y. Zhang, and H.-W. Hou, *Inorganica Chim. Acta*, 2011, **375**, 2.

25.   G. Mehlana, C. Wilkinson, G. Ramon, and S.A Bourne, *Polyhedron*, 2015, **98**, 224.

26.   J. Luo, Y. Zhao, H. Xu, T. L. Kinnibrugh, D. Yang, T. V Timofeeva, L. L. Daemen, J. Zhang, W. Bao, J. D. Thompson, and R. P. Currier, *Inorg. Chem.*, 2007, **46**, 9021.

27.   H.-L. Zhou, Y.-B. Zhang, J.-P. Zhang, and X.-M. Chen, *Nat. Commun.*, 2015, **6**, 6917.

28.   Z.-L. Wang, W.-H. Fang, and G.-Y. Yang, *Chem. Commun.*, 2010, **46**, 8216.

29.   M.-H. Zeng, Y. Tan, Y. He, Z. Yin, Q. Chen, and M. Kurmoo, *Inorg. Chem.*, 2013, **52**, 2353.

30.   G. Mehlana, S. a Bourne, and G. Ramon, *Dalton Trans.*, 2012, **41**, 4224.

31.   G. Mehlana, G. Ramon, and S. a Bourne, *CrystEngComm*, 2013, **15**, 9521.

32.   M.-H. Zeng, Y.-L. Zhou, M.-C. Wu, H.-L. Sun, and M. Du, *Inorg. Chem.*, 2010, **49**, 6436.

33.   M. Zeng, Z. Yin, Y. Tan, W. Zhang, Y. He, M. Kurmoo, M. Zeng, Z. Yin, Y. Tan, W. Zhang, and Y. He, *J. Am. Chem. Soc.*, 2014.

34.   X. Zhang, Y. Wang, Y. Song, and E. Gao, *Inorg. Chem.*, 2011, **50**, 7284.

35.   M. C. Das, H. Xu, S. Xiang, Z. Zhang, H. D. Arman, G. Qian, and B. Chen, *Chemistry*, 2011, **17**, 7817.

36.  I. Imaz, G. Mouchaham, N. Roques, S. Brandès, and J.-P. Sutter, *Inorg. Chem.*, 2013, **52**, 11237.

37.  G. Férey and C. Serre, *Chem. Soc. Rev.*, 2009, **38**, 1380.

38.  R. F. Bruinsma, P. G. De Gennes, J. B. Freund, and D. Levine, *Nature*, 2004, **427**, 523.

39.  T. Devic, C. Serre, N. Audebrand, J. Marrot, and G. Férey, *J. Am. Chem. Soc.*, 2005, **127**, 12788.

40.  S. Surblé, F. Millange, C. Serre, T. Düren, M. Latroche, S. Bourrelly, P. L. Llewellyn, and G. Férey, *J. Am. Chem. Soc.*, 2006, **128**, 14889.

41.  S. Sanda, S. Parshamoni, and S. Konar, *Inorg. Chem.*, 2013, **52**, 12866.

42.  X.-H. Jin, J.-K. Sun, L.-X. Cai, and J. Zhang, *Chem. Commun.*, 2011, **47**, 2667.

43.  G. Mehlana, S. a Bourne, and G. Ramon, *CrystEngComm*, 2014, **16**, 8160.

44.  P. G. Yot, Q. Ma, J. Haines, Q. Yang, A. Ghoufi, T. Devic, C. Serre, V. Dmitriev, G. Férey, C. Zhong, and G. Maurin, *Chem. Sci.*, 2012, **3**, 1100.

45.  F. Millange, C. Serre, N. Guillou, G. Férey, and R. I. Walton, *Angew. Chem. Int. Ed. Engl.*, 2008, **47**, 4100.

46.  Y.-S. Wei, K.-J. Chen, P.-Q. Liao, B.-Y. Zhu, R.-B. Lin, H.-L. Zhou, B.-Y. Wang, W. Xue, J.-P. Zhang, and X.-M. Chen, *Chem. Sci.*, 2013, **4**, 1539.

47.  J. C. Saint Remi, T. Rémy, V. Van Hunskerken, S. van de Perre, T. Duerinck, M. Maes, D. De Vos, E. Gobechiya, C. E. A Kirschhock, G. V Baron, and J. F. M. Denayer, *ChemSusChem*, 2011, **4**, 1074.

48.  C.-Y. Niu, X.-F. Zheng, Y. He, Z.-Q. Feng, and C.-H. Kou, *CrystEngComm*, 2010, **12**, 2847.

49.  Y. Wu, V. K. Peterson, E. Luks, T. a Darwish, and C. J. Kepert, *Angew. Chem. Int. Ed.*, 2014, **53**, 5175.

50.  I. Grobler, V. J. Smith, P. M. Bhatt, S. A. Herbert, and L. J. Barbour, *J. Am. Chem. Soc.*, 2013, **135**, 6411.

51.  C. Yang, X. Wang, and M. A. Omary, *Angew. Chemie - Int. Ed.*, 2009, **48**, 2500.

52.  L. D. Devries, P. M. Barron, E. P. Hurley, C. Hu, and W. Choe, *J. Am. Chem. Soc.*, 2011, 133, 14848.

53.  D. F. Sava, M. A. Rodriguez, K. W. Chapman, P. J. Chupas, A. Greathouse, P. S. Crozier, and T. M. Neno, *J. Am. Chem. Soc.*, 2011, **133**, 12398.

54.  B. Xin, G. Zeng, L. Gao, Y. Li, S. Xing, J. Hua, G. Li, Z. Shi, and S. Feng, *Dalton Trans.*, 2013, **42**, 7562.

55.  C. Falaise, C. Volkringer, J. Facqueur, T. Bousquet, L. Gasnot, and T. Loiseau, *Chem. Commun.*, 2013, **49**, 10320.

56.  P. Huang, C. Kuo, C. Hsieh, and Y. Horng, *Chem. Commun.*, 2012, **48**, 3227.

57.  Y.-C. He, J. Yang, G.-C. Yang, W.-Q. Kan, and J.-F. Ma, *Chem. Commun.*, 2012, **48**, 7859.

58.  J. Li, P. Huang, X.-R. Wu, J. Tao, R.-B. Huang, and L.-S. Zheng, *Chem. Sci.*, 2013, **4**, 3232.

59.  G. Mehlana, Thesis, University of Cape Town, 2014.

60.  D. F. Sava, M. A. Rodriguez, K. W. Chapman, P. J. Chupas, J. A. Greathouse, P. S. Crozier, and T. M. Nenoff, *J. Am. Chem. Soc.*, 2011, **133**, 12398.

61.  H. J. Choi and M. P. Suh, *J. Am. Chem. Soc.*, 2004, **126**, 15844.

62. L. Dobrzańska, G. O. Lloyd, H. G. Raubenheimer, and L. J. Barbour, *J. Am. Chem. Soc.*, 2006, **128**, 698.

63. B. F. Abrahams, M. Moylan, S. D. Orchard, and R. Robson, *Angew. Chemie - Int. Ed.*, 2003, **42**, 1848.

64. Z.-J. Zhang, W. Shi, Z. Niu, H.-H. Li, B. Zhao, P. Cheng, D.-Z. Liao, and S.-P. Yan, *Chem. Commun.*, 2011, **47**, 6425.

65. A.K Chaudhari, S. Mukherjee, S. S. Nagarkar, B. Joarder and S.K Ghosh, *CrystEngComm*, 2013, **15**, 9465.

66. Z.-Z. Lu, R. Zhang, Y.-Z. Li, Z.-J. Guo, and H.-G. Zheng, *J. Am. Chem. Soc.*, 2011, **133**, 4172.

67. J. Zhang, Y.-S. Xue, J. Bai, M. Fang, Y.-Z. Li, H.-B. Du, and X.-Z. You, *CrystEngComm*, 2011, **13**, 6010.

68. P.-C. Guo, T.-Y. Chen, X.-M. Ren, Z. Chu, and W. Jin, *J. Mater. Chem. A*, 2014, **2**, 13698.

69. H. Hara, A. Kobayashi, S. Noro, H.-C. Chang, and M. Kato, *Dalton Trans.*, 2011, **40**, 8012.

70. J. Cui, Y. Li, Z. Guo, and H. Zheng, *Chem. Commun.*, 2013, **49**, 555.

71. C.-Y. Sun, X.-L. Wang, C. Qin, J.-L. Jin, Z.-M. Su, P. Huang, and K.-Z. Shao, *Chemistry*, 2013, **19**, 3639.

72. T. Kern, U. Monkowius, M. Zabel, and G. Knör, *Eur. J. Inorg. Chem.*, 2010, **2010**, 4148.

73. C. Z. and X. Z. Y. Dong, J. Ma, S. Liu, *Cryst. Growth Des.*, 2013, DOI: 10.1039/C3CE41886C.

74. S. R. Miller, D. Heurtaux, T. Baati, P. Horcajada, C. Serre, and J. Grene, *Chem. Commun.*, 2010, 4526.

75. Z. Xie, L. Ma, K. E. DeKrafft, A. Jin, and W. Lin, *J. Am. Chem. Soc.*, 2010, **132**, 922.